Organic & Biomolecular Chemistry

Accepted Manuscript

This article can be cited before page numbers have been issued, to do this please use: J. Gong, C. Liu, X. Jiao, S. He, L. Zhao and X. Zeng, *Org. Biomol. Chem.*, 2020, DOI: 10.1039/D0OB00507J.

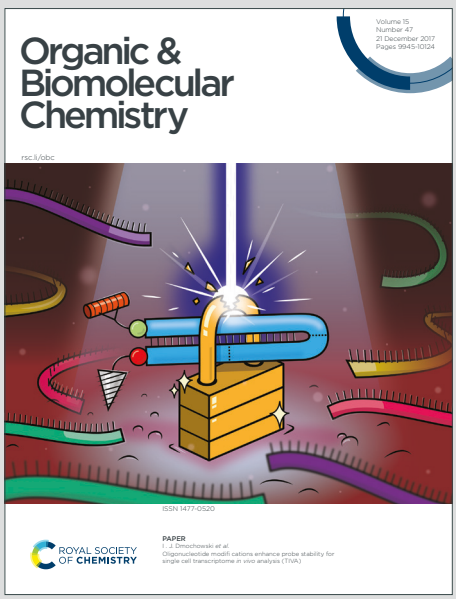

ROYAL SOCIETY OF CHEMISTRY

rsc.li/obc

View Article Online
DOI: 10.1039/D0OB00507J

ARTICLE

A novel near-infrared fluorescent probe with improved Stokes shift for specific detection of Hg^{2+} in mitochondria

Received 00th January 20xx,
Accepted 00th January 20xx

DOI: 10.1039/x0xx00000x

Jin Gong, [a] Chang Liu, [b] Xiaojie Jiao, [b] Song He, [b] Liancheng Zhao [a] and Xianshun Zeng [*,a,b]

Mercury ion (Hg^{2+}), one of the most notorious heavy metal ions, not only cause environmental pollution, but also endanger human health. There is evidence that Hg^{2+} tend to accumulate in the mitochondria and to induce apoptosis. However, mitochondria-targeted near-infrared (NIR) fluorescent probes with large Stokes shifts are still scarcely described for the specific detection of Hg^{2+}. In this work, a novel near-infrared fluorescent probe **JRQNS** with large Stokes shift (78 nm) was reported, and applied for sensitive and specific detection of Hg^{2+} in mitochondria by incorporating an additional amine group with fused rings to rhodamine dyes to enhance the electron donating ability of amine groups. As expected, the probe exhibited high selectivity and sensitivity to Hg^{2+} with detection limit as low as 1.5 nM and fast response times (3 min), revealing that **JRQNS** could be used as a practical probe for quantitative detection of Hg^{2+} in real-time. Importantly, **JRQNS** can be used as an efficient organelle-targeting probe for imaging Hg^{2+} in mitochondria of living cells, and thus detect Hg^{2+} in real-time there. The application of the probe for its selective localization in mitochondria along with the nanomolar level of limit of detection to Hg^{2+} ions provided a potential tool for studying the cytotoxic mechanisms of Hg^{2+}.

Introduction

As one of the most notorious heavy metal ions, mercury ion (Hg^{2+}) has attracted extensive attention and been considered as the primary environmental hazard in the past few decades.[1-3] Mercury species are a particular concern in many aspects due to their extremely toxicity, which are subsequently bio-accumulated through the food chain in the tissues of fish and marine mammals and eventually enter the human body.[4-6] Because mercury shows a strong affinity to sulfur-containing organic ligands, it causes the dysfunction of proteins and enzymes and results in a wide variety of diseases related to liver and kidney dysfunction, central nervous system damage, imbalance in the immune system, and even death.[7-10] Furthermore, studies had shown that Hg^{2+} tend to accumulate in the mitochondria, and induce apoptosis due to its binding to thiol-containing proteins on the mitochondrial inner membrane.[11-15] Therefore, the development of mitochondria-targeted detection tools with high selectivity and sensitivity is important for studying the cytotoxic mechanism induced by Hg^{2+}.

In recent years, small molecule fluorescent probe technology had been widely used in the detection of Hg^{2+} due to its high selectivity, high sensitivity, simplicity of implementation, real-time and in situ detection, etc.[16-30] Generally, derivatives of rhodamine were widely introduced in Hg^{2+} detection due to excellent photophysical properties, including high quantum efficiency, high photostability, excellent water solubility and biocompatibility.[31-35] However, traditional rhodamine dyes have some major drawbacks, such as the short fluorescence emission wavelength (< 600 nm) and the narrow Stokes shifts (< 30 nm), which limit their biological imaging applications due to background interference, self-quenching, excitation wavelength interference and photodamage to living cells.[31-35] To date, several strategies for increasing the emission wavelength of rhodamine dyes have been developed. Generally, extending the π-conjugated system of rhodamine scaffold is a versatile strategy for shifting the excitation/emission bands of fluorophores.[36-37] In addition, replacing the oxygen atom in the rhodamine scaffold with other atoms, including nitrogen, silicon, selenium, tellurium, sulfur, antimony, etc, is another effective strategy.[38-39] However, these strategies still bear some limitations, such as the narrow Stokes shifts, and few near-infrared (NIR) Hg^{2+} fluorescent probes with mitochondrial targeting.[40-42] Consequently, it is necessary to design and synthesize mitochondria-targeted fluorescent probes with NIR emission and large Stokes shifts for monitoring Hg^{2+} in living cells.

It is well known that the absorption and emission wavelengths of traditional rhodamine dyes are highly dependent on the substituents on the amino group. In a pioneering works, the introduction of a piperazine group in the scaffold of rhodamine could red shift the emission wavelengths by altering the intramolecular charge transfer (ICT) properties of the chomophore.[43-44] In 2013, Zhang et al. fused 4-diethyl-1,2,3,4-tetrahydroquinoxaline into rhodamine scaffold to afford

[a] School of Materials Science and Engineering, Harbin Institute of Technology, Harbin, 150001, China.
[b] Tianjin Key Laboratory for Photoelectric Materials and Devices, School of Materials Science & Engineering, Tianjin University of Technology, Tianjin, 300384, China. E-mail: xshzeng@tjut.edu.cn.

† Footnotes relating to the title and/or authors should appear here.
Electronic Supplementary Information (ESI) available: [details of any supplementary information available should be included here]. See DOI: 10.1039/x0xx00000x

new rhodamine dyes by enhancing the electron donating ability,[43] which not only red shifted the emission wavelength, but also effectively increased the Stokes shift. In 2018, Lucka and Liu et al. reported the incorporation of a piperazine fused ring on the rhodamine scaffold, which also both increased the emission wavelength and the Stokes shift.[44] In addition, the cationic xanthene moiety is normally work as a functional group for targeting mitochondria,[45] and increase the water solubility of the probe. In this work, we reported a novel mitochondria-targeted Hg^{2+} fluorescent probe **JRQNS** with NIR emission and large Stokes shift by incorporating an additional amine group with fused rings to rhodamine dyes to enhance the electron donating ability of amine groups. As expected, the probe exhibited high selectivity, high sensitivity, low detection limit (1.5 nM), and fast response time (3 minutes) for the detection of Hg^{2+} via a specific Hg^{2+}-promoted desulfurization-cyclization reaction. Gratifyingly, **JRQNS** can be accumulated in mitochondria, and thus detect Hg^{2+} in real-time there, which provided a potential tool for studying the cytotoxic mechanisms of Hg^{2+}.

Results and discussion

Synthesis of JRQNS

The fluorescent probe **JRQNS** was synthesized according to the procedures in **Scheme 1**. The intermediate compounds **1**, **2** and **3** were prepared according to the literature in high yields,[43,46-47] and the detailed reaction reagents and conditions were depicted in **Scheme 1**. By using the rearrangement reaction in the presence of methanesulfonic acid, the intramolecular ring-opened new dye **JRQ** was yielded as a blue compound (81%). With the reaction of **JRQ** and hydrazine hydrate in methanol, the key intermediate **JRQN** was obtained in 53% yield. Followed by the reaction of **JRQN** with phenyl isothiocyanate under mild condition, the probe **JRQNS** was produced in 55% yield. The structures of the new compounds

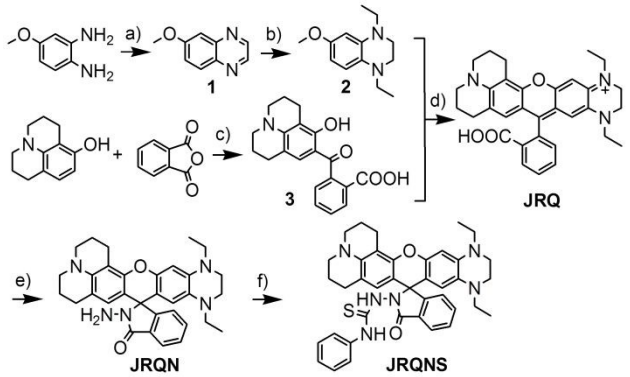

Scheme 2 Synthesis route of **JRQNS.** Reagents and conditions: a) succinaldehyde, CH_3CN, 60 °C, overnight; b) $NaBH_4$, toluene, AcOH, 5 °C to reflux, 5 h; c) toluene, reflux, overnight; d) CH_3SO_3H, 80 °C, 8 h; e) NH_2NH_2, MeOH, 50 °C, 6 h; f) phenyl isothiocyanate, DMF, 50 °C, 6 h.

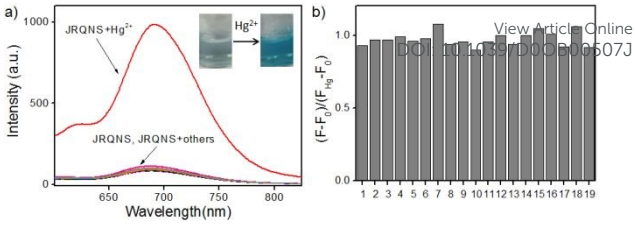

Fig. 1 a) Fluorescence spectra of **JRQNS** (10 μM) in response to 1 equiv. various metal ions. Inset: Color change of **JRQNS** in the absence/presence of Hg^{2+}; b) Fluorescence responses of **JRQNS** (10 μM) to Hg^{2+} (1 equiv.) in the presence of other metal ions (1 equiv.). Metal ions: 1) Al^{3+}; 2) Cr^{3+}; 3) Fe^{3+}; 4) Cd^{2+}; 5) Co^{2+}; 6) Mg^{2+}; 7) Cu^{2+}; 8) Fe^{2+}; 9) Ca^{2+}; 10) Pd^{2+}; 11) Zn^{2+}; 12) Hg^{2+}; 13) Pb^{2+}; 14) Ni^{2+}; 15) Mn^{2+}; 16) K^+; 17) Ag^+; 18) Li^+; 19) Na^+. The conditions: HEPES buffer (10 mM, pH = 7.4, containing 20% CH_3CN), λ_{ex} = 580 nm, slit = 5/5 nm.

JRQ, JRQN and **JRQNS** were fully characterized by NMR and HRMS, and detailed data were recorded in the supporting information.

Sensing properties of JRQNS

In order to test the *in vitro* response of **JRQNS** as a potential Hg^{2+} sensor, absorption and emission spectra were recorded in the presence of various metal ions under the same conditions, including: Al^{3+}, Cr^{3+}, Fe^{3+}, Cd^{2+}, Co^{2+}, Mg^{2+}, Cu^{2+}, Fe^{2+}, Ca^{2+}, Pd^{2+}, Zn^{2+}, Pb^{2+}, Ni^{2+}, Mn^{2+}, K^+, Ag^+, Li^+, Na^+, and Hg^{2+}. As shown in **Fig. 1a**, the fluorescence intensity of the probe at 691 nm was significantly enhanced after addition of 1 equiv. Hg^{2+}, which is significantly red shifted compared with those of conventional rhodamine dyes (~570 nm),[49] due to the electron donating ability of amine groups was enlarged after introduction of the 4-diethyl-1,2,3,4-tetrahydroquinoxaline. In contrast, biologically relevant metal ions as well as other heavy-metal ions did not afford any change in the emission spectra of **JRQNS** upon metal ion addition, indicating that Hg^{2+} specifically induced fluorescence recovery of the probe. Accordingly, when 1 equiv. Hg^{2+} ions were added, the absorption intensity of the probe at 613 nm was significantly increased, whereas no obvious changes of absorption intensity of the probe at 613 nm were observed after addition of other metal ions (**Fig. S1**). Simultaneously, upon addition of Hg^{2+}, a colorimetric change from colorless to dark blue was observed, which allowed the probe could discriminate the Hg^{2+} ions from other metal cations (inset of **Fig. 1a**). Gratifyingly, the Stokes shift of **JRQNS** was found to be 78 nm, which was obviously larger than those of conventional rhodamine dyes (< 30 nm).[49]

According to the literatures,[48] we speculated that the "turn-on" signal was initiated by Hg^{2+}-promoted desulfurization-cyclization reaction illustrated in **Fig. S2**. In the absence of Hg^{2+}, **JRQNS** mainly kept a non-fluorescent spirocyclic form. The absorbance over 400 nm and the fluorescence emission at 691 nm are very weak. In the presence of Hg^{2+}, however, the Hg^{2+}-elicited desulfurization-cyclization reaction of the probe led to the intense absorption at 613 nm and the fluorescence emission at 691 nm. To verify the speculated mechanism, HRMS was conducted to analyze the molecular weight of the probe after the reaction with Hg^{2+}. As shown in **Fig. S2**, an intense peak at m/z 623.3126 corresponding to **JRQNS-OX** was distinct after the reaction of

JRQNS with Hg^{2+}, suggesting that the Hg^{2+}-promoted desulfurization-cyclization reaction of the probe is correct. To further understand the sensing mechanism, the ^1H NMR titration experiments of **JRQNS** with Hg^{2+} were conducted in DMSO-d_6 (**Fig. S3**). Upon addition of Hg^{2+}, two broad singlet of thiourea group at δ 9.31 (H_a) and 8.71 (H_b) ppm completely disappeared. Also, the aromatic protons H_c, H_e and H_f were shifted upfield and H_d was shifted downfield after the addition of Hg^{2+}. These results basically supported our speculative sensing mechanism. Furthermore, in order to confirm the stoichiometry between the Hg^{2+} and **JRQNS**, a Job's plot was conducted (**Fig. S4**). The fraction of the maximum absorbance of Hg^{2+} at 613 nm is 0.5, indicating that the binding formation of stoichiometry is 1:1.

Subsequently, in order to further evaluate the selectivity of **JRQNS** towards Hg^{2+}, the competition experiments were performed in which Hg^{2+} ions were added to **JRQNS** upon addition of 1 equiv. physiologically and environmentally relevant potentially interfering metal ions under the same condition. As shown in **Fig. 1b**, all of the tested interfering metal ions had minor or no interference with signal response to Hg^{2+}, indicating that the presence of interfering ions did not affect the selective identification of the probe. Therefore, the selectivity and competition experiments results suggested that **JRQNS** displayed excellent selectivity toward Hg^{2+} which afforded an *OFF-ON* signal response, and could even expand the potential applications in bioimaging related fields.

In order to further evaluate the sensitivity of the probe towards Hg^{2+}, thus, the continuous titration experiment was conducted by using UV/Vis and fluorescence spectroscopy. As shown in **Fig. 2a**, upon addition of increasing concentration of Hg^{2+} (0-1.1 equiv.) to the solution, the fluorescence intensity of the probe at 691 nm gradually increased and reached the plateau at 1 equiv., which could be attributed to the Hg^{2+}-induced desulfurization-cyclization reaction. The binding constant derived from the fluorescence titrations was found to be 1.35×10^6 M^{-1} based on 1:1 stoichiometry.[50] Subsequent data analysis revealed an excellent linear relationship (R = 0.9990) between the fluorescence intensity of **JRQNS** at 691 nm and the concentration of Hg^{2+} in the range of 0 to 2.5 μM (**Fig. 2b**). The detection limit of Hg^{2+} is determined to be 1.5 nM based on the equation of $3\sigma/k$,[51-52] where k is the slope plotted from the fluorescence intensity at 691 nm versus the concentration of Hg^{2+}, and σ is the relative standard deviation for 10 parallel fluorescence measurements of the blank solution without Hg^{2+}. Compared with some of the other small molecule fluorescent probes for detecting Hg^{2+}, the detection limit of **JRQNS** was at a relatively low level, and **JRQNS** exhibited lager Stokes shift and faster response times (**Table S1**). The detection limit of **JRQNS** was far lower than the U.S. EPA's (Environmental Protection Agency) limit on drinking water (9.97 nM).[53] Similarly, upon addition of increasing concentration of Hg^{2+} (0-1.1 equiv.) to the solution, the absorption intensity at 613 nm gradually increased and reached the plateau when the accumulated amount of Hg^{2+} reached 1 equivalents (**Fig. S5**). Continuous titration experiments revealed that **JRQNS** showed high sensitivity to

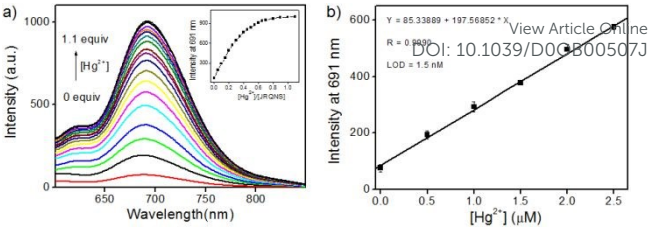

Fig. 2 a) Fluorescence spectra of **JRQNS** (10 μM) in the presence of different concentrations of Hg^{2+} (0–1.1 equiv.); Inset: fluorescence intensity changes as a function of Hg^{2+} concentration; b) The linear relationship between the emission intensity and Hg^{2+} concentrations (0-2.5 μM); The conditions: HEPES buffer (10 mM, pH = 7.4, containing 20% CH_3CN), λ_{ex} = 580 nm, slit = 5/5 nm.

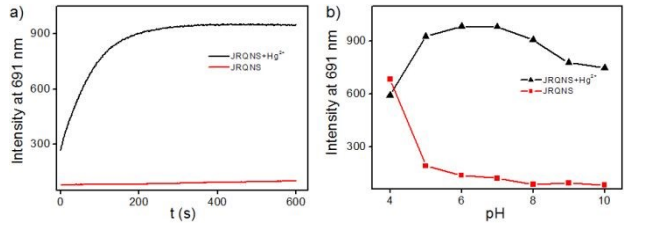

Fig. 3 a) Time-dependence fluorescence intensity of **JRQNS** (10 μM) upon addition of 10 μM Hg^{2+}; b) Fluorescence intensity of **JRQNS** (10 μM) as a function of pH value in the absence/presence of Hg^{2+} (10 μM); The conditions: HEPES buffer (10 mM, pH = 7.4, containing 20% CH_3CN), λ_{ex} = 580 nm, slit = 5/5 nm.

Hg^{2+} and could be used as a practical probe for quantitative detection Hg^{2+} in drinking water.

In addition, in order to assess the possibility of real-time detection, we investigated the response time of the probe towards Hg^{2+}. In the absence of Hg^{2+}, the fluorescence intensity at 691 nm was maintained at the initial value and no obvious change occurred within 10 minutes (**Fig. 3a**), indicating that **JRQNS** could be stably present in the solution and owned high photo-stability. In contrast, after adding 1 equiv. of Hg^{2+}, the fluorescence intensity at 691 nm increased rapidly and reached a plateau within 3 minutes (**Fig. 3a**), indicating that **JRQNS** could be used as an effective candidate for monitoring Hg^{2+} in real-time. At the same time, for practical applicability in more complicated systems, the response of the probe in the absence and presence of Hg^{2+} at different pH values were evaluated. In the absence of Hg^{2+}, the probe exhibited weak fluorescence under alkaline conditions due to the spirocyclic form, while high fluorescence was observed under acidic conditions for ring-opening induced by H^+ (**Fig. 3b**). Upon addition of Hg^{2+}, the fluorescence intensity at 691 nm increased significantly over a pH range of 5-10 (**Fig. 3b**) due to the ring-opening induced by Hg^{2+}, indicating that **JRQNS** can be utilized as a Hg^{2+} selective probe over a wide pH range. Above results suggested that **JRQNS** was qualified for the real-time detection of trace amount of Hg^{2+} in the physiological environment.

Fluorescence imaging of JRQNS

Since **JRQNS** shows rapid response time, high photo-stability, excellent selectivity and sensitivity, it is possible to explore the potential applications of the probe for sensing Hg^{2+} in living cells. Before that, it is crucial to evaluate the

View Article Online
DOI: 10.1039/D0OB00507J

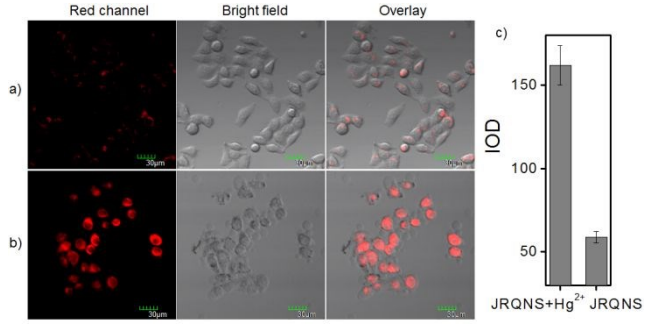

Fig.4 Fluorescence images of HeLa cells. a) Cells were incubated with **JRQNS** (0.1 μM) for 30 min; b) and then incubated with Hg^{2+} (0.1 μM) for another 30 min; c) Histogram of fluorescence enhancement. λ_{ex} = 559 nm, λ_{em} = 647-747 nm.

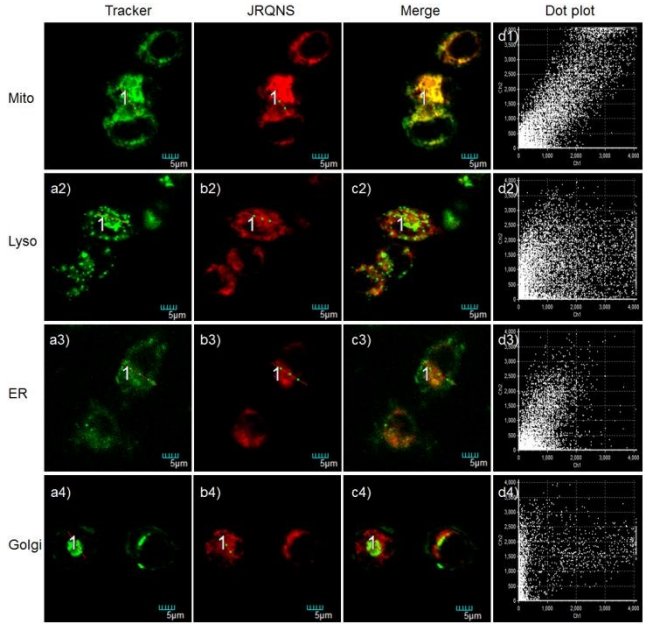

Fig.5 Fluorescence imaging of HeLa cells costained with **JRQNS** (100 nM) upon treatment of and Mito-Tracker Green (200 nM), Lyso-Tracker Green Green (200 nM), ER-Tracker Green (200 nM), or Golgi-Tracker Green (200 nM). Cells were incubated with probes at 37 °C for 30 min, and then treated with Hg^{2+} (100 nM) for another 30 min, and finally washed before imaging. a) Costained with Mito-Tracker Green; b) Costained with Lyso-Tracker Green, c) Costained with ER-Tracker Green; d) Costained with Golgi-Tracker Green. Red channel: λ_{ex} = 559 nm, λ_{em} = 664-764 nm. Green channel: λ_{ex} = 488 nm, λ_{em} = 511-534 nm.

cytotoxicity of **JRQNS** to living cells by a well-established MTT assay. **Fig. S6** depicted the viability of HeLa cells under various probe concentrations from 0 μM to 20 μM. The results demonstrate that more than 80% of cells are viable, showing the low toxicity of the probe to cultured cells under experimental conditions and inferring their potential use in intracellular imaging of living cells. Then, bioimaging applications of **JRQNS** for monitoring of Hg^{2+} in living cells were carried out using HeLa cells. As shown in **Fig. 4a**, the probe showed weak fluorescence signals under the red channel, confirming the extremely low background of the probe. In contrast, after the addition of Hg^{2+} and then incubation for another 30 min under the same conditions, strong fluorescence signals of the probe under the red channel (**Fig. 4b**) was observed. Compared with the untreated cells, the relative enhancement of fluorescence signals is about 3-fold (**Fig. 4c**). Thus, above-described results obviously revealed that the probe had good membrane permeability and could be used for imaging Hg^{2+} in living cells.

By carefully observing the overlay images of the red channel and the bright field, we found that the distribution of the fluorescence signals in the cells unevenly fill the entire cytoplasm, but concentrated in some regions, implied that **JRQNS** was likely to target organelles. As described above, Hg^{2+} mainly accumulates in the mitochondria,[54-56] and the xanthene dyes leads to the proactive accumulation in mitochondria,[45] thereby **JRQNS** is highly likely to accumulate in mitochondria. Furthermore, NIR fluorescent probes for detection of Hg^{2+} in mitochondria are still rarely reported,[40-42] which greatly prompted us to further explore the localization properties of the probe. To explore the targeting-organelle of **JRQNS**, **JRQNS** was co-cultured with commercially available trackers Mito-Tracker Green, Lyso-Tracker Green, ER-Tracker Green, and Golgi-Tracker Green, respectively, and then cultured with Hg^{2+}. As shown in **Fig. 5a**, the fluorescence signals of **JRQNS** completely overlapped with the fluorescence signals of Mito and yellow pixels in the overlay image were observed, indicating that **JRQNS** distributed predominantly in mitochondria. In particular, high Pearson's coefficient (0.93) and overlap coefficient (0.93) indicated that the staining of **JRQNS** fitted well with that of Mito. In contrast, the other overlay images showed that the fluorescence signals of **JRQNS** and the fluorescence signals of other trackers (Lyso, ER, or Golgi) were clearly distributed in different regions (**Fig. 5b-d**). Similarly, the lower Pearson's coefficients and overlap coefficients showed that the fluorescence signals of **JRQNS** and other trackers were essentially not distributed in the same regions, indicating that **JRQNS** fitted not co-localize exactly with other organelles. These results indicated that **JRQNS** can be used as an efficient organelle-targeting probe for imaging Hg^{2+} in mitochondria of living cells, which provided a potential tool for studying the cytotoxicity of Hg^{2+}.

Conclusions

In summary, we developed a novel near-infrared (691 nm) fluorescent probe **JRQNS** with large Stokes shift (78 nm) by integrating an additional amine group with fused rings to rhodamine dyes to increase the electron donating ability of amine groups. As expected, **JRQNS** exhibited high selectivity and sensitivity to Hg^{2+} with detection limit as low as 1.5 nM and fast response times (3 min), revealing that **JRQNS** could be used as a practical probe for quantitative detection of Hg^{2+} in real-time. Importantly, due to the cationic and lipophilic characters of the xanthene moiety, the probe is mitochondria targetable. **JRQNS** could permeate cell membranes and accumulate in the mitochondria, and thus detect Hg^{2+} in real-time there, which provided a potential tool for studying the cytotoxic mechanisms of Hg^{2+}.

Experimental

View Article Online DOI: 10.1039/D0OB00507J

Instruments and reagents

In this paper, all reagents and organic solvents were commercially available in analytical grade, and were used directly without further purification unless otherwise stated. The structures of the compounds were confirmed by NMR and HRMS spectrometry. ^{1}H NMR (400 MHz) and ^{13}C NMR (100 MHz) spectra were collected by Bruker spectrometer using tetramethylsilane (TMS) as an internal standard. Chemical shift (δ) values are expressed in ppm and coupling constants are expressed in Hz. HRMS were measured by Agilent 6510 Q-TOF LC/MS instrument (Agilent Technologies, Palo Alto, CA). Spectroscopic properties were collected by F-4600 fluorescence spectrophotometer (Hitachi Japan) and UV-2550 UV/Vis spectrophotometer (Hitachi Japan). The pH was measured using a FE 20/EL 20 pH meter (Mettler-Toledo Instruments (Shanghai) CO., Ltd.). Cell imaging was performed by Olympus FV 1000-IX81 laser scanning confocal imaging.

Preparation of stock solutions

Stock solutions (10 mM) of the nitrate salts of Al^{3+}, Cr^{3+}, Fe^{3+}, Cd^{2+}, Co^{2+}, Mg^{2+}, Cu^{2+}, Fe^{2+}, Ca^{2+}, Pd^{2+}, Zn^{2+}, Pb^{2+}, Ni^{2+}, Mn^{2+}, K^+, Ag^+, Li^+, Na^+, and Hg^{2+} ions were prepared in distilled water. Stock solutions of **JRQNS** (5 mM) were prepared in DMF. Test solutions were prepared by placing appropriate volume of the stock solution into a 5 mL vial, adding an appropriate aliquot of each metal stock, and diluting the solution to 3 mL with CH_3CN/HEPES (2/8, v/v). Unless otherwise stated, all data were collected at 10 min after the addition of guest ions.

Synthesis

The key intermediate compounds **1**, **2** and **3** were prepared according to the literature.[43,46-47]

Synthesis of JRQ:

The compound **2** (2.2 g, 10 mmol) and **3** (3.7 g, 11 mmol) were dissolved in 5 mL methanesulfonic acid, and then the reaction system was heated to 80 °C and reacted under vigorous stirring for 8 hours. After cooling to room temperature, the mixture was extracted with DCM (50 mL × 3) and the collected organic layers were dried over anhydrous Na_2SO_4. The crude product was obtained by concentration under vacuum, and then purified by column chromatography (DCM/MeOH, 15/1, v/v) to afford the compound **JRQ** as a blue solid (4.1 g) in 81% yield. ^{1}H NMR (400 MHz, $CDCl_3$) δ 8.35 – 8.25 (m, 1H), 7.54 – 7.47 (m, 2H), 7.07 – 7.01 (m, 1H), 6.67 (s, 1H), 6.59 (s, 1H), 5.96 (s, 1H), 3.61 (s, 2H), 3.55 (dd, *J* = 14.2, 7.1 Hz, 2H), 3.42 – 3.37 (m, 4H), 3.19 (s, 2H), 3.07 – 2.91 (m, 4H), 2.64 – 2.51 (m, 2H), 2.02 (d, *J* = 5.0 Hz, 2H), 1.87 (d, *J* = 5.7 Hz, 2H), 1.28 (t, *J* = 7.1 Hz, 3H), 0.87 (t, *J* = 7.2 Hz, 3H). ^{13}C NMR (100 MHz, $CDCl_3$) δ 166.59, 155.76, 153.64, 151.59, 149.71, 146.43, 134.50, 134.42, 133.19, 131.65, 131.24, 129.41, 129.38, 125.79, 123.50, 114.85, 113.87, 104.64, 104.05, 94.41, 50.72, 50.26, 48.02, 47.02, 45.43, 44.04, 27.72, 20.72, 20.05, 19.89, 10.99, 9.42. HRMS m/z = 508.2600 calcd for $C_{32}H_{34}N_3O_3$ $[M]^+$, found: 508.2609.

Synthesis of JRQN:

Hydrazine hydrate (50 μL) was added to the methanol solution (10 mL) of **JRQ** (1.02 g, 2 mmol), and then the reaction system was heated to 50 °C and reacted under vigorous stirring for 6 hours. After cooling to room temperature, the mixture was extracted with DCM (50 mL × 3) and the collected organic layers were dried over anhydrous Na_2SO_4. The crude product was obtained by concentration under vacuum, and then purified by column chromatography (DCM/MeOH, 8/1, v/v) to afford the compound **JRQN** as a pale yellow solid (0.55 g) in 53% yield. ^{1}H NMR (400 MHz, $CDCl_3$) δ 7.96 – 7.87 (m, 1H), 7.46 – 7.36 (m, 2H), 7.14 – 7.04 (m, 1H), 6.34 (s, 1H), 6.03 (s, 1H), 5.62 (s, 1H), 3.56 (d, *J* = 0.6 Hz, 2H), 3.40 – 3.29 (m, 4H), 3.13 (d, *J* = 7.6 Hz, 4H), 3.11 – 3.05 (m, 2H), 3.03 – 2.85 (m, 4H), 2.49 (qd, *J* = 15.9, 7.9 Hz, 2H), 2.08 – 1.98 (m, 2H), 1.86 (dt, *J* = 12.0, 6.2 Hz, 2H), 1.20 (t, *J* = 7.0 Hz, 3H), 0.83 (t, *J* = 7.0 Hz, 3H). ^{13}C NMR (100 MHz, $CDCl_3$) δ 166.25, 151.98, 149.03, 146.21, 143.53, 137.27, 132.32, 131.40, 129.79, 127.83, 123.94, 123.88, 122.87, 117.19, 107.70, 104.34, 104.24, 97.86, 66.90, 49.97, 49.51, 46.65, 45.74, 45.43, 45.35, 27.20, 22.02, 21.48, 21.28, 10.51, 9.61. HRMS m/z = 522.2895 calcd for $C_{32}H_{35}N_5O_2$ $[M+H]^+$, found: 522.2886.

Synthesis of JRQNS:

Phenyl isothiocyanate (203 mg, 1.5 mmol) was added to the DMF solution (10 mL) of **JRQN** (521mg, 1 mmol), and reacted under an argon atmosphere at 50 °C for 6 hours. After cooling to room temperature, the mixture was extracted with DCM (50 mL × 3) and the collected organic layers were dried over anhydrous Na_2SO_4. The crude product was obtained by concentration under vacuum, and then purified by column chromatography (DCM/EtOAc, 20/1, v/v) to afford the compound **JRQNS** as a pale yellow solid (361 mg) in 55% yield. ^{1}H NMR (400 MHz, $CDCl_3$) δ 8.01 (d, *J* = 7.4 Hz, 1H), 7.62 (d, *J* = 6.6 Hz, 2H), 7.59 – 7.53 (m, 1H), 7.20 (t, *J* = 7.6 Hz, 2H), 7.07 – 7.12 (m, 3H), 6.35 (s, 1H), 6.00 (s, 1H), 5.55 (s, 1H), 3.39 – 3.31 (m, 3H), 3.14 (dd, *J* = 11.8, 7.5 Hz, 3H), 3.08 (dd, *J* = 10.8, 6.0 Hz, 2H), 3.05 – 3.01 (m, 1H), 3.00 – 2.95 (m, 1H), 2.93 – 2.83 (m, 3H), 2.77 (dt, *J* = 14.2, 7.1 Hz, 1H), 2.50 – 2.34 (m, 2H), 2.05 – 1.98 (m, 2H), 1.80 (dt, *J* = 13.2, 7.0 Hz, 2H), 1.26 (t, *J* = 7.1 Hz, 3H), 1.21 (t, *J* = 7.0 Hz, 3H). ^{13}C NMR (100 MHz, $CDCl_3$) δ 167.32, 150.75, 149.46, 146.57, 144.14, 137.74, 134.07, 132.16, 128.99, 128.81, 128.24, 128.21, 125.07, 125.00, 124.96, 124.89, 124.67, 124.39, 117.63, 108.06, 106.00, 103.69, 130.64, 98.09, 49.83, 49.43, 46.65, 45.61, 45.39, 45.34, 27.32, 21.77, 21.25, 21.16, 14.21, 10.46, 9.74. HRMS m/z = 657.3011 calcd for $C_{39}H_{41}N_6O_2S^+$ $[M+H]^+$, found: 657.3017.

Standard MTT assay

HeLa cells were inoculated with a 96-well plate and allowed to adhere for 12 hours. After changing the culture medium, different concentrations of **JRQNS** (0, 1, 3, 5, 10, and 20 μM) were separately added to the cells and cultured for another 24 hours to allow them to fully enter the cells. The culture solution was changed and washed three times with PBS, and then 3-(4,5-dimethylthiazol-2-yl)-2,5-diphenyltetrazolium bromide was added to each well and cultured for another 4 hours. The culture solution was removed and added DMSO, and then the absorbance at 490 nm was measured after standing for 2 hours.

Cell culture and fluorescence imaging

HeLa cells for imaging were cultured in DMEM medium supplemented with 10% (v/v) fetal bovine serum and penicillin/streptomycin (100 μg/mL) in an atmosphere of 5% CO_2 at 37 °C. The cells were cultured for 2 hours to adhere them to the 12-well plate, and then subjected to fluorescence imaging experiments. The cells were incubated with 0.1 μM **JRQNS** for 30 minutes, and then Hg^{2+} (0.1 μM) was added and incubated for another 30 minutes. For co-localization experiments, **JRQNS** (100 nM) were incubated with a 200 nM trackers (Golgi-Tracker Green (Golgi), Mito-Tracker Green (Mito), ER-Tracker Green (ER), and Lyso-Tracker Green (Lyso)) for 30 minutes, respectively, and then treated with Hg^{2+} (100 nM) for another 30 min. Fluorescence imaging was performed after washing the medium three times with PBS buffer.

Conflicts of interest

There are no conflicts to declare.

Acknowledgements

This work was sponsored by the National Natural Science Foundation of China (NNSFC 21907075; 21272172), and the Natural Science Foundation of Tianjin City (19JCZDJC32400; 18JCQNJC75900).

Notes and references

1 M. F Wolfe, S. Schwarzbach and R. A. Sulaiman, *Environ. Toxicol. Chem.,* 1998, **17**, 146.
2 D. Zeller and S. Booth, *Science*, 2005, **310**, 777.
3 F. D. Natale, A. Lancia, A. Molino, M. D. Natale, D. Karatza and D. Musmarra, *J. Hazard. Mater.,* 2006, **132**, 220.
4 C. R. Baum, *Curr. Opin. Pediatr.,* 1999, **11**, 265.
5 M. Harada, *Crit. Rev. Toxicol.,* 1995, **25**, 1.
6 A. M. L. Kraepiel, K. Keller, H. B. Chin, E. G. Malcolm and F. M. M. Morel, *Environ. Sci. Technol.,* 2003, **37**, 5551.
7 P. B. Tchounwou, W. K. Ayensu, N. Ninashvili and D. Sutton, *Environ. Toxicol*., 2003, **18**, 149.
8 D. W. Boening, *Chemosphere*, 2000, **40**, 1335.
9 M. McNutt, *Science*, 2013, **341**, 1442.
10 A. Renzoni, F. Zino and E. Franchi, *Environ. Res.*, 1998, **77**, 68.
11 N. Sone, M. K. Larsstuvold and Y. Kagawa, *J. Biochem.*, 1977, **82**, 859.
12 T. Toimela and H. Tahti, *Arch. Toxicol.*, 2004, **78**, 565.
13 A. C. Santos, S. A. Uyemura, N. A. G. Santos, F. E. Mingatto and C. Curti, *Mol. Cell Biochem.*, 1997, **177**, 53.
14 P. B. Pal, S. Pal, J. Das and P. C. Sil, *Amino. Acids.,* 2012; **42**: 1669.
15 A. Tonazzi, N. Giangregorio, L. Console, M. Scalise, D. L. Russa, C. Notaristefano, E. Brunelli and D. Barca, Indiveri C., *Chem. Res. Toxicol.,* 2015, **28**, 1015.
16 E. M. Nolan and S. J. Lippard, *Chem. Rev.*, 2008, **108**, 3443.
17 H. N. Kim, W. X. Ren, J. S. Kim and J. Yoon, *Chem. Soc. Rev*., 2012, **41**, 3210.
18 Y. Yang, Q. Zhao, W. Feng and F. Li, *Chem. Rev.*, 2013, **113**, 192.
19 Y. Tang, D. Lee, J. Wang, G. Li, J. Yu, W. Lin and J. Yoon, *Chem. Soc. Rev.,* 2015, **44**, 5003.
20 D. Wu, A. C. Sedgwick, T. Gunnlaugsson, E. U. Akkaya, J. Yoon and T. D. James, *Chem. Soc. Rev.,* 2017, **46**, 7105.
21 S. Wu, W. Tu, Y. Zhao, X. Wang, J. Song and X. Yang, *Anal. Chem.*, 2018, **90**, 14423.
22 Q. Duan, H. Zhu, C. Liu, R. Yuan, Z. Fang, Z. Wang, P. Jia, Z. Li, W. Sheng and B. Zhu, *Analyst*, 2019, **144**, 1426.
23 L. Chen, S. J. Park, D. Wu, H. M. Kim and J. Yoon, *Chem. Commun*., 2019, **55**, 1766.
24 L. Li, Y. Wen, L. Xu, Q. Xu, S. Song, X. Zuo, J. Yan, W. Zhang and G. Liu, *Biosens. Bioelectron*., 2016, **75**, 433.
25 Y. Y. Liu, S. Naha, N. Thirumalaivasan, S. Velmathi and S. P. Wu, *Sens. Actuators. B Chem.*, 2018, **277**, 673.
26 S. Li, D. Huang, J. Wan, S. Yan, J. Jiang and H. Xiao, *Sens. Actuators. B Chem.,* 2018, **275**, 101.
27 Y. Zhang, H. Chen, D. Chen, D. Wu, Z. Chen, J. Zhang, X. Chen, S. Liu and J. Yin, *Sens. Actuators. B Chem.*, 2016, **224**, 907.
28 Y. Shan, W. Yao, Z. Liang, L. Zhu, S. Yang, Z. Ruan, *Dyes. Pigment.,* 2018, **156**, 1.
29 J. Tang, H. Wu, S. Yin and Y. Han, *Tetrahedron. Lett.*, 2019, **60**, 541.
30 B. Zhou, S. Qin, B. Chen and Y. Han, *Tetrahedron. Lett*., 2018, **59**, 4359.
31 M. Beija, C. A. M. Afonso and J. M. G. Martinho, *Chem. Soc. Rev.*, 2009, **38**, 2410.
32 L. Yuan, W. Lin, K. Zheng and S. Zhu, *Acc. Chem. Res*., 2013, **46**, 1462.
33 H. Zhu, J. Fan, B. Wang and X. Peng, *Chem. Soc. Rev.*, 2015, **44**, 4337.
34 G. Sivaraman, M. Iniya, T. Anand, N. G. Kotla, O. Sunnapu, S. Singaravadivel, A. Gulyani and D. Chellappa, *Coord. Chem. Rev.*, 2018, **357**, 50.
35 B. Kaur, N. Kaur, S. Kumar, *Coord. Chem. Rev.*, 2018, **358**, 13.
36 E. David, J. Lejeune, R. S. Pellet, J. Schulz, M. Lemaire and J. Chauvin, *Tetrahedron. Lett.*, 2008, **49,** 1860.
37 C. Liu, X. Jiao, Q. Wang, K. Huang, S. He, L. Zhao and X. Zeng, *Chem. Commun*., 2017, **53**, 10727.
38 Y. Koide, Y. Urano, K. Hanaoka, T. Terai and T. Nagano, *J. Am. Chem. Soc.*, 2011, **133**, 5680.
39 W. Piao, K. Hanaoka, T. Fujisawa, S. Takeuchi, T. Komatsu, T. Ueno, T. Terai, T. Tahara, T. Nagano and Y. Urano, *J. Am. Chem. Soc.,* 2017, **139**, 13713.
40 H. Agarwalla, P. S. Mahajan, D. Sahu, N. Taye, B. Ganguly, S. B. Mhaske, S. Chattopadhyay and A. Das, *Inorg. Chem*., 2016, **55**, 12052.
41 J. Chen, W. Liu, B. Zhou, G. Niu, H. Zhang, J. Wu, Y. Wang, W. Ju and P. Wang, *J. Org. Chem.*, 2013, **78**, 6121.
42 L. Lei, X. Tan, S. Luo and C. Shi, *New. J. Chem.,* 2017, **41**, 8899.
43 Z. Tian, B. Tian and J. Zhang, *Dyes. Pigment.,* 2013, **99**, 1132.
44 H. Liu, Y. Zhang, S. Xia, M. Fang, W. Mazi, Y. Zeng, T. Johnston, A. Pap and R. L. Luck, *Chem. Commun.,* 2018, **54**, 7625.
45 Y. K. Kim, H. H. Ha, J. S. Lee, X. Bi, Y. H. Ahn, S. Hajar, J. J. Lee and Y. T. Chang, *J. Am. Chem. Soc.,* 2010, **132**, 576.
46 E. A. Belyaeva, D. Dymkowska, M. R. Wieckowski and L. Wojtczak, *Toxicol. Appl. Pharmacol*., 2008, **231**, 34.
47 E. A. Belyaeva, T. V. Sokolova, L. V. Emelyanova and I. O. Zakharova, *Sci. World J.*, 2012, **2012**, 1.
48 S. K. Yao, Y. Qian, Z. Qi, C. Lu and Y. Cui, *New J. Chem.*, 2017, **41**, 13495.
49 M. Beija, C. A. M. Afonso and J. M. G. *Chem. Soc. Rev.,* 2009, **38**, 2410.
50 P. Laurent, H. Miyaji, S. R. Collinson, I. Prokeš, C. J. Moody, J. H. R. Tucker and A. M. Z. Slawin, *Org. Lett.*, 2002, **4**, 4037.
51 M. Shortreed, R. Kopelman, M. Kuhn and B. Hoyland, *Anal. Chem.,* 1996, **68**, 1414.
52 A. Caballero, R. Martinez, V. Lloveras, I. Ratera, J. Vidal-Gancedo, K. Wurst, A. Tárraga, P. Molina and J. Veciana, *J. Am. Chem. Soc.,* 2005, **127**, 15666.

View Article Online
DOI: 10.1039/D0OB00507J

53 Mercury Update: Impact of Fish Advisories, EPA Fact Sheet EPA-823-F-01-011; EPA, Office of Water: Washington, DC, 2001.
54 S. Kamino, M. Murakami, M. Tanioka, Y. Shirasaki, K. Watanabe, J. Horigome, Y. Ooyama and S. Enomoto, *Org. Lett.,* 2014, **16**, 258.
55 A. R. Jagtap, V. S. Satam, R. N. Rajule and V. R. Kanetkar, *Dyes. Pigment*., 2009, **82**, 84.
56 M. Konigsberg, N. E. López-Díazguerrero, L. Bucio and M. C. Gutierrez-Ruiz, *J. Appl. Toxicol.*, 2001, **21**, 323.